Applied Mathematics and Computation 000 (2018) 1–17

Contents lists available at ScienceDirect

Applied Mathematics and Computation

journal homepage: www.elsevier.com/locate/amc

Modeling electrochemical transport of ions in the molten CaF_2–FeO slag operating under a DC voltage

E. Karimi-Sibaki [a], A. Kharicha [a,b,*], M. Wu [a,b], A. Ludwig [b], J. Bohacek [b]

[a] Christian-Doppler Laboratory for Advanced Process Simulation of Solidification and Melting, Montanuniversitaet of Leoben, Franz-Josef-Str. 18, A-8700 Leoben, Austria
[b] Chair of Simulation and Modeling of Metallurgical Processes, Montanuniversitaet of Leoben, Franz-Josef-Str. 18, A-8700 Leoben, Austria

ARTICLE INFO

Article history:
Available online xxx

Keywords:
Numerical modeling
Poisson–Nernst–Planck (PNP) equations
Electroslag remelting (ESR)
Electric potential
Faradaic reaction
Ferrous ion

ABSTRACT

Electrically resistive CaF_2-based slags are extensively used in many metallurgical processes such as electroslag remelting (ESR). Chemical and electrochemical reactions as well as transport of ions in the molten slag (electrolyte) are critical phenomena for those processes. In this paper, an electrochemical system including two parallel, planar electrodes and a completely dissociated electrolyte operating under a DC voltage is modeled. The transport of ions by electro-migration and diffusion is modeled by solving the Poisson–Nernst–Planck (PNP) equations using the Finite Volume Method (FVM). The non-linear Butler–Volmer equations are implemented to describe the boundary condition for the reacting ions at the electrode–electrolyte interface. Firstly, we study a binary symmetrical electrolyte, which was previously addressed by Bazant et al. (2005), to verify the numerical model. Secondly, we employed the model to investigate our target CaF_2–FeO system. The electrolyte is consisted of reacting (Fe^{2+}) and non-reacting (Ca^{+2}, O^{2-}, F^{-}) ions. Spatial distributions of concentrations of ions, charge density, and electric potential across the electrolyte at steady state are analyzed. It is found that the Faradaic reaction of the ferrous ion (Fe^{2+}) has negligible impact on the electric potential field at very low current density (<1 A m^{-2}). The strong impact of electric double layer (EDL) capacitance on the system behavior is addressed throughout our analysis. Furthermore, a linear relationship among activation (surface) overpotential and current density (<1600 A m^{-2}) is observed. The simulation results helps to explain some phenomena observed in the ESR process. The higher melt rate for an anodic ESR electrode than a cathodic one is linked to the interfacial potential drop. It is found that the anodic potential drop near the anode is larger than the cathodic voltage drop near the cathode. The results are tested against an experiment.

1. Introduction

Technological applications of electrochemical phenomena in fuel cells and batteries, sensors, as well as extracting and refining of metals are rapidly growing. Molten oxides typically made of SiO_2, CaO, or Al_2O_3 are considered in molten oxide electrolysis (MOE) for metal extraction [1]. On the other hand, calcium fluoride (CaF_2)-based electrolytes, typically composed of CaF_2, Al_2O_3, CaO, SiO_2, FeO, and MgO, are frequently used in metallurgical refining processes such as electroslag remelting (ESR). The molten electrolyte, called slag, is served to protect the liquid metal against surrounding air, to remove sulfur and

* Corresponding author at: Chair of Simulation and Modeling of Metallurgical Processes, Montanuniversitaet of Leoben, Franz-Josef-Str. 18, A-8700 Leoben, Austria.
E-mail address: abdellah.kharicha@unileoben.ac.at (A. Kharicha).

https://doi.org/10.1016/j.amc.2018.01.008
0096-3003/

non-metallic inclusions from the alloy, and to provide heat through Joule heating into the process. A high degree of chemical reactivity and low electrical conductivity are desirable properties of CaF_2-based slags. An ionic or mixed ionic/electronic mechanism was postulated concerning the mode of conduction in the slag [2]. Over the past decades, the mechanism of ion conduction was addressed in numerous monographs. Mitchell and Beynon [3] used the galvanostatic pulsing technique to evaluate the concentration overpotential at the interface between an iron electrode and CaF_2-based slags. By adding a small amount of alumina to molten calcium fluoride, the electrical conductivity was found to decrease significantly. The formation of large complex ions such as $AlOF^{-}{}_2$ decreased the mobility of F^- and consequently resulted in a decrease in electrical conductivity [4]. Kojima et al. [5] have pointed out relationships between the distribution of oxygen in the ESR ingot, the electrode polarity, and the current mode (AC or DC). The melt rate of an electrode-positive (anodic) was reported to be higher than the electrode-negative (cathodic) for an ESR process operating under DC current [6,7]. Furthermore, the electrical behavior of metallic droplets which are formed at the tip of melting electrode could be influenced by electrochemical reactions. Kharicha et al. [8,9] stated that metallic droplets which were surrounded by the resistive slag could conduct an electric current when potential drops at their extremities surpassed the associated electrochemical overpotential. Contributions of electrochemical reactions taking place at the slag–metal interface were recognized to be an important factor in cleanness and refinement of the alloy. For instance, oxidation loss of alloy elements such as Ti and Al during DC operation of ESR process was reported by Etienne [10]. Additionally, Minh and King [11] postulated a diffusion-controlled electrochemical reaction for the sulfur removal from the alloy in the ESR process. Evidently, the aforementioned phenomena in the ESR process are related to the ionic properties of the slag. Therefore, it is of great importance for fundamental and technical reasons to establish an electrochemical model that includes the response of ions to the applied electric field in the slag.

Previously, kinetic Monte Carlo and phase-field models were proposed to investigate cathode shape and topology change in electrolysis [12]. The governing equations required the thermodynamic statement of free energy or entropy. In the present study, we employ the well-established Finite Volume Method (FVM) to solve the governing conservation equations known as Poisson–Nernst–Planck (PNP). The proposed model has the following key features. Mass conservations of inert (non-reacting) ions are automatically satisfied by using the FVM method. The model is not restricted to the number of involving ions (reacting or non-reacting). Furthermore, the model has a promising future to incorporate advection since FVM is the common approach to model flow field in a process.

Recently, we developed a one-dimensional model to investigate the electrochemical behavior of pure molten CaF_2 electrolyte subjected to a DC electric field [13]. The computational domain included two planar, parallel electrodes which are separated by a completely dissociated electrolyte. In the current study, we extended our model by incorporating Faradaic reactions. Firstly, the response of an arbitrary binary symmetric electrolyte (Z^+Z^-) to the applied electric field was investigated. Previously, the DC response of this electrochemical system was analyzed by Bazant et al. [14] and Chu and Bazant [15]. Here, this calculation was repeated to verify our numerical model by capturing key features of potential, concentration or charge density fields at different DC voltage. Secondly, we applied the model to study the system CaF_2–FeO in which the ferrous ion (Fe^{2+}) participated in Faradaic reactions. The influence of the applied DC voltage on the electric potential and concentration fields was investigated. Furthermore, the relationship between the applied voltage with calculated current density and overpotential was analyzed. Here, the proposed model is solely developed to study the slag composed of CaF_2–FeO. Based on the modeling results, we put forward a possible explanation for the relation between the polarity (positive or negative) and melt rate of electrode in the ESR process. The main goal is to achieve some fundamental understanding of electrochemical behavior of the fully dissociated CaF_2–FeO slag under the influence of an applied DC voltage.

2. Theory

To begin our theoretical study, we require a firm mathematical model to explain the electrochemical transport of ions in the bulk of the electrolyte. Furthermore, a mathematical description must be provided for Faradaic reactions which occur at the electrode–electrolyte interface.

2.1. Transport of ions

The Poisson–Nernst–Planck (PNP) equations describe fluxes of ions through the electrolyte which is subjected to an electric field.

$$-\nabla \cdot (\varepsilon_s \nabla \phi) = F \sum z_i c_i \tag{1}$$

$$\frac{\partial c_i}{\partial t} = -\nabla \cdot \vec{N}_i \tag{2}$$

$$\vec{N}_i = \vec{u} c_i - D_i \nabla c_i - \frac{F z_i D_i \nabla \phi}{RT} c_i \tag{3}$$

The Poisson equation, Eq. (1), describes the relationship between the electric potential (ϕ) and charge density ($\rho = F\Sigma z_i c_i$) where ε_s denote the electric permittivity of the electrolyte. Furthermore, the charge density is dependent on the Faraday constant (F) as well as concentration (c_i) and charge number (z_i) of ith ion. The total flux of ith ion (N_i) including convection,

Please cite this article as: E. Karimi-Sibaki et al., Modeling electrochemical transport of ions in the molten CaF_2–FeO slag operating under a DC voltage, Applied Mathematics and Computation (2018), https://doi.org/10.1016/j.amc.2018.01.008

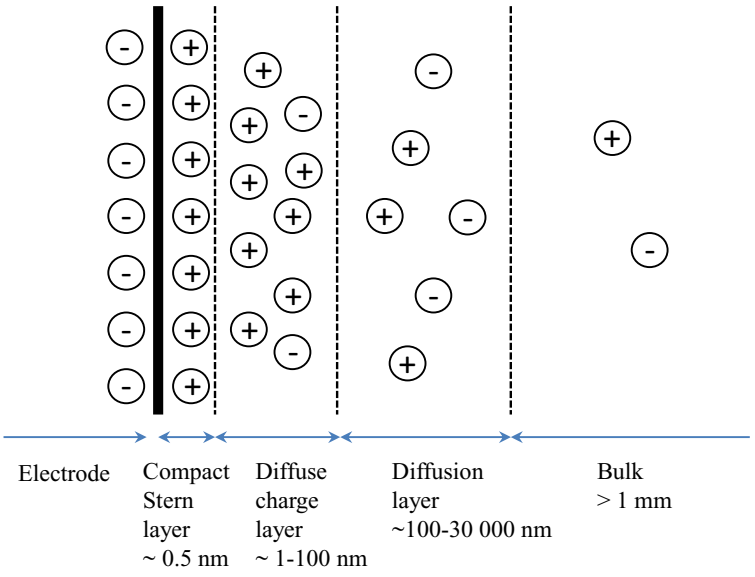

Fig. 1. Schematic representation of the structure of electric double layer (EDL).

diffusion, and electro-migration must be conserved according to Eq. (2). The convection and diffusion fluxes are dependent on the velocity ($\vec{u}$) and diffusion coefficient (D_i). Additionally, the electro-migration contributes to the transport of electroactive (non-zero charge number) ions as described in Eq. (3) where R and T are universal gas constant and temperature, respectively.

Considering a symmetric binary electrolyte, Golovnev and Trimper [16] presented the steady state solution of the PNP equations in terms of Jacobi elliptic functions. It was demonstrated that the net charge exists in a thin boundary layer (~1–100 nm) near the electrode called the diffuse charge layer. The length of the layer is known as the Debye screening length (λ_D) and expressed as,

$$\lambda_D = \sqrt{\frac{\varepsilon_s RT}{2z^2F^2c_b}} \tag{4}$$

where c_b is the bulk concentration of ions.

Theoretically, the accumulation of charge density occurs in a specific region near the electrode called electric double layer (EDL). The EDL is composed of a diffusion layer, a diffuse charge layer, and the compact Stern layer where ions are adsorbed to the surface of electrode as illustrated in Fig. 1. The motion of ions is restricted inside the extremely thin (~0.1–1 nm) compact layer. Note that, a net charge density exists in the diffuse charge layer where the electro neutrality condition is not valid. The diffusion layer is electrically neutral, whereas the concentration of ions within this layer may differ from the bulk concentration [17]. The thickness of diffusion layer where the concentration of an ion asymptotically reaches the bulk concentration is dependent on the operating condition [18].

The formulation of the problem is not complete before assigning the appropriate boundary conditions to determine a solution to the PNP equations as presented in the following section.

2.2. Kinetics of electrode reactions

Here, we assume that a general reduction-oxidation reaction takes place at the surface of electrode in which O is the oxidized species which is reduced to R,

$$O + ne^- \leftrightarrows R \tag{5}$$

In mathematical point of view, electrochemical reactions are the source/sink of ion flux into/out of the electrolyte. An equation known as “Butler–Volmer” had been suggested to describe the relationship between the reaction rate, current density, and the state of the electrically neutral bulk [17]. Typically, Arrhenius temperature dependent terms are used to describe reaction rates,

$$r(c_O, c_R, \Delta\phi_s) = k_c c_O \exp\left(-\frac{\alpha_c nF\Delta\phi_s}{RT}\right) - k_a c_R \exp\left(\frac{\alpha_a nF\Delta\phi_s}{RT}\right) \tag{6}$$

The net flux of reacting ions (r) is calculated based on the difference between rates of forward and backward reactions those in turn are influenced by concentration of reacting ions (c_o, c_R), and the voltage drop across the Stern layer ($\Delta\phi_s$).

Please cite this article as: E. Karimi-Sibaki et al., Modeling electrochemical transport of ions in the molten CaF_2–FeO slag operating under a DC voltage, Applied Mathematics and Computation (2018), https://doi.org/10.1016/j.amc.2018.01.008

Eq. (6) involves several constants such as cathodic and anodic reaction rates (k_c, k_a) as well as cathodic and anodic charge transfer coefficients (α_c, α_a). The charge transfer coefficient is bounded between zero and one. The coefficient indicates the favorable direction for the reaction, Eq. (5), whether reactant-like or product-like. The sum of cathodic and anodic charge transfer coefficients must be equal to one. Typically, similar values are chosen ($\alpha_c = \alpha_a = 0.5$) for single electron transfer reactions [17]. Eventually, the current density at the interface between electrolyte and electrode is given by,

$$j = zF\left[k_c c_O \exp\left(-\frac{\alpha_c zF\Delta\phi_s}{RT}\right) - k_a c_R \exp\left(\frac{\alpha_a zF\Delta\phi_s}{RT}\right)\right] \tag{7}$$

The rates of forward and backward reactions are equal at equilibrium, and there is no net Faradaic reaction. As such, an exchange current density can be defined that includes the rate of forward/backward reactions and concentration of reactants,

$$j_0 = F(k_c c_O^*)^{\alpha_a}(k_a c_R^*)^{\alpha_c} \tag{8}$$

Furthermore, the difference in the voltage drop across the Stern layer at equilibrium (in the absence of current) and during passage of current is defined as surface (activation) overpotential ($\eta = \Delta\phi_s - \Delta\phi_s^{eq}$). Assume that the concentrations of reactive species at electrode surface do not change from their equilibrium values ($c_o = c_o^*$ and $c_R = c_R^*$) during the operation. This can be achieved by stirring the solution or performing the experiment at low current density [17]. Ultimately, Eq. (7) could be re-written in terms of exchange current density and surface overpotential as described by Chu [19],

$$j = j_0\left[\exp\left(\frac{(1-\alpha)nF\eta}{RT}\right) - \exp\left(-\frac{\alpha nF\eta}{RT}\right)\right] \tag{9}$$

This formulation helps us to sidestep the problem of experimentally determining the concentrations of reactive species at the electrode surface. The exchange current density and surface overpotential in Eq. (9) can be estimated experimentally.

A linear relationship between the over potential and potential drop across the compact Stern layer was proposed [20–22],

$$\eta = -\lambda_s \nabla\phi \tag{10}$$

The correlation coefficient is referred as the effective Stern layer width (λ_s). Principally, the compact Stern layer acts like a nonlinear capacitor in series with the diffuse layer. λ_s represents the capacitance of the EDL that will be further described in Section 4.2.

3. General modeling

3.1. Basic equations

To facilitate the discussion, we present the relevant equations for an arbitrary binary symmetrical electrolyte (Z^+Z^-). Previously, this system was analyzed by Bazant et al. [14] and Chu and Bazant [15]. They reformulated the standard PNP equations using arithmetic means of the charge density and concentration to derive a more symmetrical form of the PNP [14,15]. In the present study, we repeated the calculation using our numerical model which directly solves the standard PNP equations. The aim is to demonstrate the capability of our model for capturing the behavior of the electrochemical system. Furthermore, this preliminary calculation helps us to improve our knowledge regarding to the influence of modeling and operational parameters such as applied voltage or exchange current density on the response of system. The electrolyte is assumed to be stagnant ($\vec{u} = 0$) and confined by two parallel planer electrodes which are separated at sufficiently large distance. Therefore, it is appropriate to formulate the PNP equations together with their boundary conditions in a one-dimensional model. The dimensionless form of the PNP equations for the binary electrolyte are given by,

$$\frac{\partial}{\partial x}\left(-\zeta^2\frac{\partial\phi^*}{\partial x}\right) = z_+C_+ + z_-C_- \tag{11}$$

$$\frac{\partial C_+}{\partial t} = \frac{\partial}{\partial x}\left(D_+\frac{\partial C_+}{\partial x} + z_+D_+C_+\frac{\partial\phi^*}{\partial x}\right) \tag{12}$$

$$\frac{\partial C_-}{\partial t} = \frac{\partial}{\partial x}\left(D_-\frac{\partial C_-}{\partial x} + z_-D_-C_-\frac{\partial\phi^*}{\partial x}\right) \tag{13}$$

The basic variables are scaled as follow,

$$\phi^* = \frac{F\phi}{RT},\ C_\pm = \frac{c_\pm}{C_{ref}},\ \zeta = \frac{\lambda_D}{L_{ref}}$$

Where $C_\pm$ is the dimensionless concentration of cation (+) or anion (−), and C_{ref} denotes the reference concentration which is typically in the same order as the concentration of ions in the bulk. Furthermore, ζ denotes the ratio of Debye

Please cite this article as: E. Karimi-Sibaki et al., Modeling electrochemical transport of ions in the molten CaF_2–FeO slag operating under a DC voltage, Applied Mathematics and Computation (2018), https://doi.org/10.1016/j.amc.2018.01.008

screening length to the reference length (L_{ref}) that is usually chosen to be the distance between electrodes. The chosen value of ζ can influence the distribution of charge density or electric potential that will be further discussed in Section 3.2.

The proper boundary conditions at each electrode are discussed in the following. The cathode is located at $x=0$, and the anode is located at $x=L$. Without loss of generality, assume that only the cation (Z^+) is reacting, and the anion (Z^-) is inert. The first pair of boundary conditions specifies the normal total flux to zero at each electrode, since the anion (Z^-) does not participate in any Faradaic reaction,

$$D_- \frac{\partial C_-}{\partial x}(0) + z_- D_- C_-(0) \frac{\partial \phi^*}{\partial x}(0) = 0 \tag{15}$$

$$D_- \frac{\partial C_-}{\partial x}(L) + z_- D_- C_-(L) \frac{\partial \phi^*}{\partial x}(L) = 0 \tag{16}$$

Only the cation (reacting ion) contributes to the current density flowing through the electrochemical cell at the steady state. Thus, the normal total flux of the cation is related to the current density,

$$D_+ \frac{\partial C_+}{\partial x}(0) + z_+ D_+ C_+ \frac{\partial \phi^*}{\partial x}(0) = -\frac{j}{z_+ C_{ref} F} \tag{17}$$

$$D_+ \frac{\partial C_+}{\partial x}(L) + z_+ D_+ C_+ \frac{\partial \phi^*}{\partial x}(L) = +\frac{j}{z_+ C_{ref} F} \tag{18}$$

Following Bazant et al. [14], the voltage drop across the Stern layer, Eq. (10), is taken into account to specify the boundary conditions for the Poisson equation (Eq. (11)),

$$\phi^*(0) = -\frac{F}{2RT}\left[V_{app} + \lambda_s \frac{\partial \phi}{\partial x}(0)\right] \tag{19}$$

$$\phi^*(L) = +\frac{F}{2RT}\left[V_{app} - \lambda_s \frac{\partial \phi}{\partial x}(L)\right] \tag{20}$$

where V_{app} is the operational voltage of the electrochemical cell. The potentiostatic condition [14,17] is applied in our model. In other words, the voltage (V_{app}) is given and the current density (j) is computed in a self-consistent way. Eventually, current density (j) and overpotential (η) can be easily evaluated using Eqs. (9) and (10). It must be stated that the calculated current density (j) is influenced by the modeling parameters such as λ_s which will be further described in Section 4.2.

3.2. Numerical solution

In the present paper, we carry out the numerical solution for a medium-sized computational domain (1 mm) to include the EDL near electrodes and the bulk of electrolyte in our calculation. Theoretically, our model is not limited to the size of system which can be relatively large (several centimeters). Consider that, with the increase of the size of domain, the total number of mesh element also increases. Consequently, the computational domain may contain several hundred thousands of mesh elements for a large scale system that requires a huge amount of computational time. Here, the total number of mesh elements is 1000. Furthermore, a variable sized mesh is used considering a very fine mesh adjacent to electrodes (minimum cell size ~30 nm) to resolve the boundary layer where the gradient is large. The size of computational cells is gradually increased away from the electrodes toward the bulk of electrolyte (maximum cell size ~5 μm) using the successive ratio of one percent [13]. The required modeling equations as well as their boundary conditions are implemented into the commercial software ANSYS-Fluent v.14.5 using User-Defined Functions (UDF). The governing equations are discretized both in time and space. The first-order implicit method is used in time. The spatial discretization is obtained by the third-order MUSCL scheme that accounts for the variable grid sizes [23]. As reported by Bazant et al. [24], it is not possible to fulfill all the boundary conditions assuming a negligible screening length compared to the size of electrochemical cell ($\zeta \sim 10^{-6}$). Physically, this assumption is consistent with the bulk electro neutrality ($\rho \sim 0$) that is always violated at the vicinity of electrode especially within the diffuse charge layer. Therefore, using a rather large value of ζ is essential to emphasize the role of diffuse charge layer and to achieve a numerical solution. For instance, ζ must be chosen as large as 0.05 to capture the asymptotic behavior of a micro electrochemical cell [24]. Aiming at further clarification of the contribution of ζ, the distribution of charge density for Z^+Z^- electrochemical system at fixed operational voltage and in absence of any Faradaic reaction is illustrated in Fig. 2. The charge density is expected to be accumulated in the very thin region near the electrodes ($\sim$ 10 nm), and the bulk of electrolyte is expected to remain neutral ($\rho = 0$). Obviously, the bulk electro neutrality condition is better satisfied using smaller ζ, e.g. 10^{-5}. In the current study, transient calculation is made but only final steady state results are analyzed. All parameters used in our calculations are listed in Table 1.

Please cite this article as: E. Karimi-Sibaki et al., Modeling electrochemical transport of ions in the molten CaF_2–FeO slag operating under a DC voltage, Applied Mathematics and Computation (2018), https://doi.org/10.1016/j.amc.2018.01.008

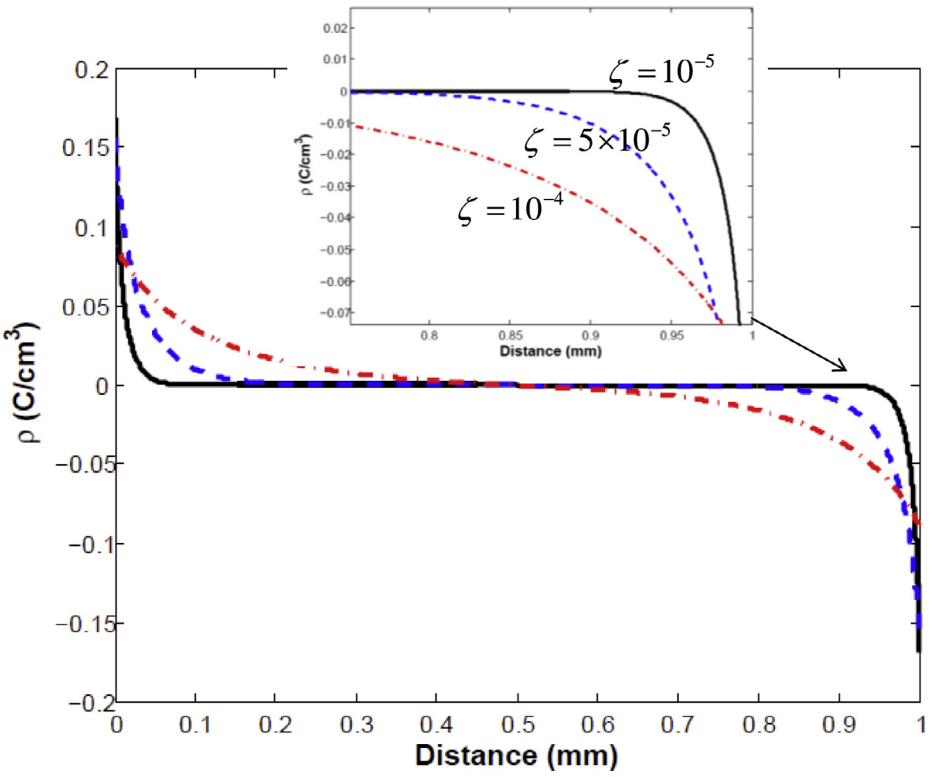

Fig. 2. The charge density at steady state for ZZ electrochemical system is plotted across the electrolyte blocked by cathode ($x = 0$) and anode ($x = 1$). Numerical results for different values of ζ are compared. Insert shows a zoomed area near the anode.

3.3. Parameter study

The effect of exchange current density on the electrochemical behavior of the system Z^+Z^-subjected to a constant DC voltage (0.1 V) is indicated in Fig. 3. Only the cation (Z^+) reacts, and the anion is inert (Z^-). The injection of the cation at the anode and the removal of cation at the cathode can alter the concentration field in the electrochemical cell. As such, the concentration of cation is not known a priori. Once the voltage is applied, the anion accumulates near the anode, whereas the cation departs from the anode and moves toward the cathode. The variation in the concentration fields of cation and anion under the effect of exchange current density (reaction rate) is illustrated in Fig. 3(c). A linear concentration profile of the cation develops in the bulk. Obviously, the slope of the linear part of the concentration profile increases as the diffuse charge layer expands into the bulk at large presumed exchange current density (e.g. 10^9 A m^{-2}). Additionally, the total concentration of ions near the anode significantly increases due the increase of injection rate of the cation. In contrast, the overall concentration of ions remarkably decreases at high removal rate (e.g. $j_0 = 10^9$ A m^{-2}) of the cation near the cathode. Similarly, a larger slope of electric potential profile is obtained at higher exchange current density as a consequence of the aforementioned expansion that is shown in Fig. 3(a). Furthermore, the bulk expectedly remains electroneutral as shown in Fig. 3(b).

The operational voltage has also a crucial effect on the field structure of the electrochemical cell. Essentially, the concentration of ions near the cathode may approach to zero once the voltage exceeds a critical value [17]. There exists a limiting-current to guarantee that the concentration of the cation (current carrier) remains non-negative within the cell. In the absence of excess of supporting electrolytes (non-reacting ions), the space charge layer in the vicinity of EDL is significantly expanded to the bulk as illustrated in Fig. 4(b).

The space charge layer observed near the cathode is a transition layer in which the bulk concentration of ions becomes very small, whereas the concentration of the cation at the surface of cathode becomes significantly large as shown in Fig. 4(c). The intense deposition of the cation at the surface of cathode notably decreases the potential drop in the Stern layer that in turn permits the current density to go beyond the limiting current [15]. Therefore, anodic and cathodic boundary layers do not evenly contribute to the potential field. The cell voltage strongly diverges near the cathode in order to sustain a current larger than the limiting value as illustrated in Fig. 4(a).

Although the presented results are valid mathematical solutions of the standard equations, their physical relevance must be carefully scrutinized under extreme conditions such as super limiting current. One should consider that the standard PNP equations are intended to describe an infinitely dilute solution in a relatively small electric field [17]. In the past,

Please cite this article as: E. Karimi-Sibaki et al., Modeling electrochemical transport of ions in the molten CaF_2–FeO slag operating under a DC voltage, Applied Mathematics and Computation (2018), https://doi.org/10.1016/j.amc.2018.01.008

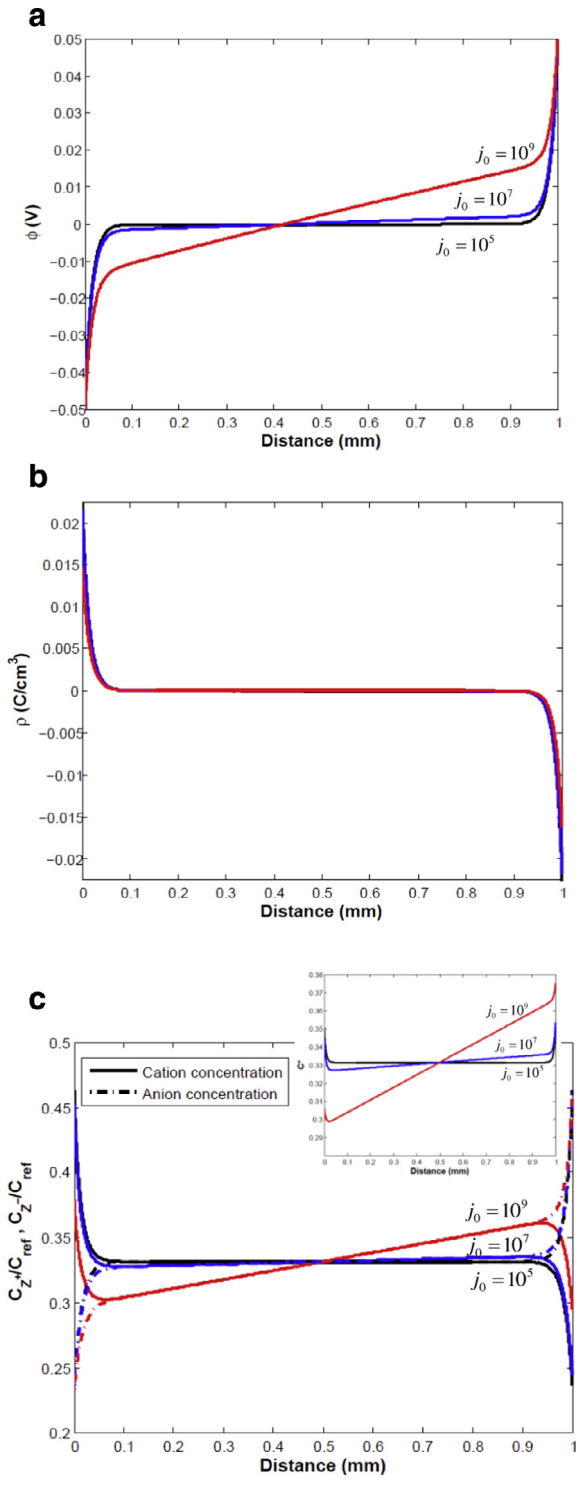

Fig. 3. Numerical results for different values of the exchange current density (j_0) are compared. The following parameters are plotted across the electrolyte (ZZ) blocked by cathode ($x = 0$) and anode ($x = 1$) at fixed operational voltage ($V_{app} = 0.1$ V): (a) electric potential, (b) charge density, (c) the dimensionless concentrations of the cation (Z^+) and anion (Z^-). Insert in (c) shows the sum of the dimensionless concentrations of the cation and anion.

Please cite this article as: E. Karimi-Sibaki et al., Modeling electrochemical transport of ions in the molten CaF_2–FeO slag operating under a DC voltage, Applied Mathematics and Computation (2018), https://doi.org/10.1016/j.amc.2018.01.008

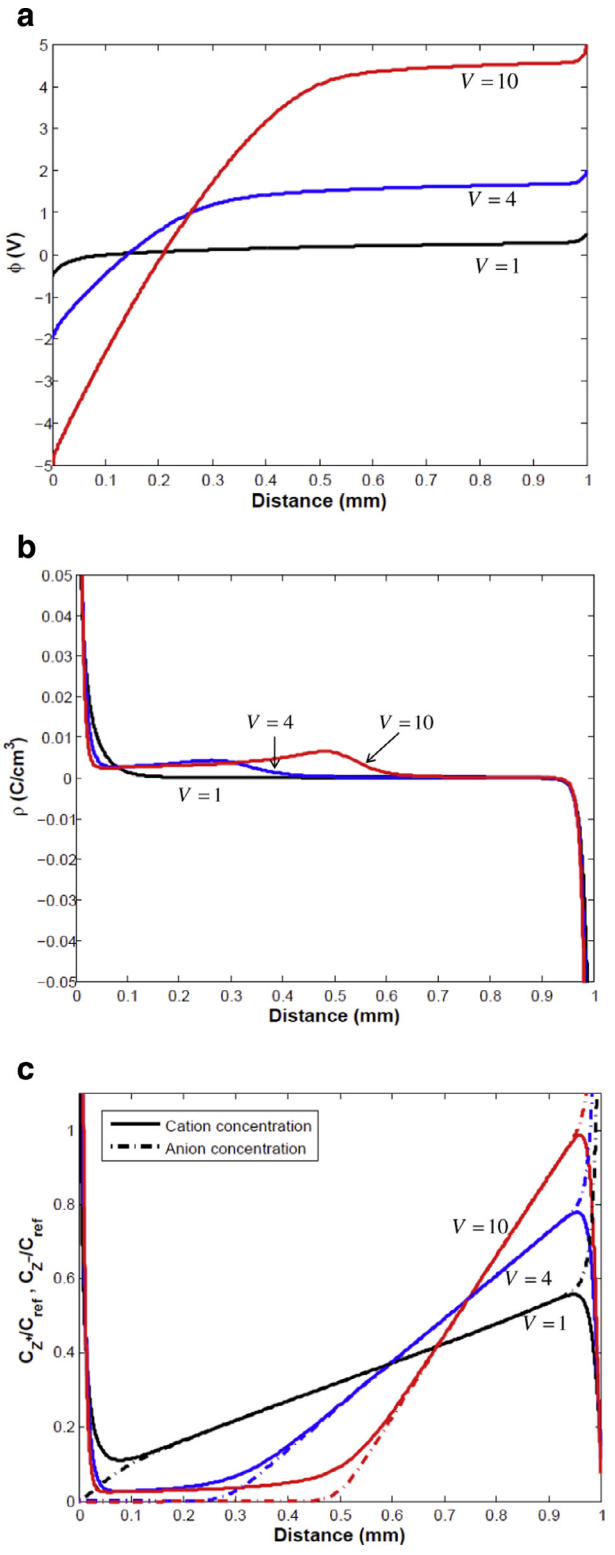

Fig. 4. Numerical results for different values of the operational voltage (V_{app}) are compared. The following parameters are plotted across the electrolyte (ZZ) confined by cathode ($x = 0$) and anode ($x = 1$) at fixed exchange current density ($j_0 = 10^9$ A m^{-2}): (a) electric potential, (b) charge density, (c) the dimensionless concentrations of the cation (Z^+) and anion (Z^-).

Please cite this article as: E. Karimi-Sibaki et al., Modeling electrochemical transport of ions in the molten CaF_2–FeO slag operating under a DC voltage, Applied Mathematics and Computation (2018), https://doi.org/10.1016/j.amc.2018.01.008

Table 1
Parameters used for our calculations of two electrochemical systems: one with ZZ electrolyte, and another with CaF_2–FeO electrolyte.

Parameter	
T: Bulk temperature (K)	1723 [34]
R: Universal gas constant (J mol^{-1} K^{-1})	8.314546
F: Faraday constant (A s mol^{-1})	96,485
ε_s: Electric permittivity (F m^{-1})	8.85418×10^{-12}
C_{ref}: Reference concentration (mol m^{-3})	1×10^{5}
L_{ref}: Reference length (m)	1×10^{-3}
j_0: Exchange current density (A m^{-2})	4×10^{4} [34]
λ_D: Debye length (m)	1×10^{-9}
λ_s: Effective Stern length (m)	Variable [Table 2]
α: Charge transfer coefficient	0.6 [34]
ζ	1×10^{-5}
ZZ electrolyte	
Z^+: Concentration (mol m^{-3})	0.333×10^{5}
Z^+: Diffusion coefficient (m^2 s^{-1})	4×10^{-9}
Z^+: Charge number	+1
Z^-: Concentration (mol m^{-3})	0.333×10^{5}
Z^-: Diffusion coefficient (m^2 s^{-1})	4×10^{-9}
Z^-: Charge number	−1
CaF_2–FeO electrolyte	
Ca^{2+}: Concentration (mol m^{-3})	0.333×10^{5}
Ca^{2+}: Diffusion coefficient (m^2 s^{-1})	5.66×10^{-9} [33]
Ca^{2+}: Charge number	+2
F^-: Concentration (mol m^{-3})	0.666×10^{5}
F^-: Diffusion coefficient (m^2 s^{-1})	4.12×10^{-9} [33]
F^-: Charge number	−1
Fe^{2+}: Concentration (mol m^{-3})	8.96 [34]
Fe^{2+}: Diffusion coefficient (m^2 s^{-1})	2.5×10^{-9} [34]
Fe^{2+}: Charge number	+2
O^{2-}: Concentration (mol m^{-3})	8.96 [34]
O^{2-}: Diffusion coefficient (m^2 s^{-1})	2.5×10^{-9} [34]
O^{2-}: Charge number	−2

the existence and impacts of expanded space charge layer on the electrochemical behavior of a cell were mathematically analyzed by researchers [15,25–27]. The expanded space charge layer could also impact the flow field in the electrolyte. For instance, the action of electric field on the expanded space charge layer causes electro-convective instability near a permselective membrane as reported by Pham et al. [28]. It was claimed that the presence of expanded space charge layer was confirmed in nanoscale film of silicon oxide used in micro batteries [29]. However, a relatively high amount of current is required to reach the limiting-current regime for large scale electrochemical systems.

The presented results in this section for the ZZ electrochemical system are used to demonstrate the capability of our model for capturing relevant electrochemical responses to a DC voltage. In addition, they are useful for pedagogical purposes to clarify important electrochemical terms such as exchange current density, space charge layer, etc. For further information, the interested readers are highly encouraged to consult with the original study given in Refs. [14,15].

4. Calculation of CaF_2–FeO system

4.1. The system description and configuration

A schematic representation of the electrochemical system including CaF_2–FeO slag and iron electrodes is shown in Fig. 5. For the sake of simplicity, and to avoid extra complexity, the following assumptions for the model are made:

(i) The slag is assumed to remain stagnant ($\vec{u} = 0$). Therefore, the transport of ions by advection is neglected.
(ii) Formation of oxyfluorides and complexation of metal ions which may take place in the molten slag are not included in the model [30].
(iii) The slag is assumed to be fully dissociated into its component ions,

$$CaF_2 \rightarrow Ca^{2+} + 2F^- \tag{21}$$

$$FeO \rightarrow Fe^{2+} + O^{2-} \tag{22}$$

Please cite this article as: E. Karimi-Sibaki et al., Modeling electrochemical transport of ions in the molten CaF_2–FeO slag operating under a DC voltage, Applied Mathematics and Computation (2018), https://doi.org/10.1016/j.amc.2018.01.008

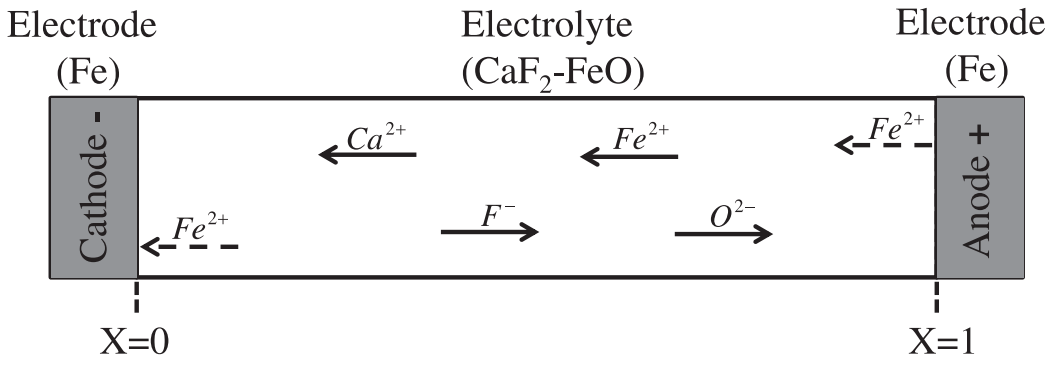

Fig. 5. The electrochemical system including CaF_2–FeO slag and iron electrodes is schematically shown. The electrolyte is fully dissociated, and only ferrous ion (Fe^{2+}) participates in Faradaic reactions.

The initial concentration of CaF_2–FeO system is given in Table 1. The concentration of CaF_2 is calculated by dividing the density (2600 kg m^{-3}) to molecular weight (78.07 g mol^{-1}). According to Eq. (21), the concentration of F^- is twice larger than the concentration of Ca^{2+}.

(iv) The electric permittivity of the electrolyte is assumed to be identical to free space permittivity, since it is unknown at the high temperature of the system (1723 K).

(v) Electronic conduction through the slag is commonly reported [31,32]. Here, it is assumed that the current is only carried by the movement of ions, thus any possible electric conduction is ignored.

(vi) Impacts of the state (liquid or solid) of the electrode on the overall behavior of the system are ignored. The electrode–electrolyte interface is considered as the boundary of the computational domain. Therefore, no calculation is carried out in the bulk of electrode.

(vii) Ca^{2+}, F^-, and O^{2-} are non-reacting ions, whereas the ferrous ion (Fe^{2+}) participates in the Faradaic reactions. Special care must be taken in specifying the boundary condition for the ferrous ion to ensure the mass conservation. Oxidation of iron, Eq. (23), takes place at the anode to form the soluble ferrous ion. In terms of modeling, the ferrous ion is injected into the electrolyte at the anode (Eq. (23)), thus a positive mass flux of the ferrous ion at the anode is specified. Correspondingly, a negative mass flux of the ferrous ion at the cathode is considered, as the ferrous ion is removed from the electrolyte at the cathode (Eq. (24)). We ignore the neutral iron (Fe) in our calculations.

$$\text{(At anode): } Fe \rightarrow Fe^{2+} + 2e^- \tag{23}$$

$$\text{(At cathode): } Fe^{2+} + 2e^- \rightarrow Fe \tag{24}$$

(viii) Previously, Mitchell and Beynon [3] suggested that at relatively high current density the ferrous ion (Fe^{2+}) may convert to the ferric (Fe^{3+}) ion due to enrichment of ferrous ion at the anode. They concluded that oxidation of the iron at the anode, Eq. (23), and reduction of ferrous ion (Fe^{2+}) at the cathode, Eq. (24), are the governing redox reactions at low current density below ca. 2 kA m^{-2} [3]. Thus, any validation effort for comparing the model estimates against experiment results must be limited to the low applied current density (<2 kA m^{-2}).

As shown in the Fig. 5, the ferrous ion is injected into the electrolyte at the anode, and removed from the electrolyte at the cathode.

Here, the conservation equations (Nernst–Planck) for the system CaF_2–FeO are not written to avoid redundancy. The transport of positive ions such as Ca^{2+} and $Fe^{2+}$are described by Eq. (12). Furthermore, the transport of negative ions like O^{2-} and F^- are expressed by Eq. (13). All required parameters for our calculations are extracted from Refs. [33,34]. These involving ions have dissimilar constant parameters such as diffusion coefficient which are listed in Table 1. The experimental uncertainties associated with many of the diffusion coefficient values reported in the literature are large. Numerous parameters such as temperature, pressure, slag composition, radius and valency of diffusing species can affect diffusion coefficient values [35]. The diffusion and migration (both dependent on the diffusion coefficient) are competing against each other. In terms of mathematical modeling (Eqs. (12) and (13)), any change in the magnitude of the diffusion coefficient influences both the migration and diffusion fluxes. Aiming at achieving the steady state and ignoring the advective transport of ions (Eqs. (12) and (13)), the diffusion coefficients has no influence on the total flux of non-reacting ions (O^{2-}, F^-, and Ca^{2+}). On the other hand, the diffusion coefficient of the reacting ion (Fe^{2+}) can influence the relationship between the applied voltage and current density. The system can carry higher amount of current density with the increase of diffusion coefficient of the reacting ion (Fe^{2+}) at fixed applied voltage.

A total number of four conservation equations are solved in a coupled manner to determine concentration fields for each ion. In addition, the electric potential is coupled to the ion conservation equations via the Poisson equation, Eq. (11).

Please cite this article as: E. Karimi-Sibaki et al., Modeling electrochemical transport of ions in the molten CaF_2–FeO slag operating under a DC voltage, Applied Mathematics and Computation (2018), https://doi.org/10.1016/j.amc.2018.01.008

Table 2
Calculated relationship between applied voltage, effective Stern width, δ, magnitude of activation overpotential (positive for cathode and negative for anode) and current density for the system CaF_2–FeO electrolyte with fixed average concentration of ferrous ion within the electrolyte (8.96 mol m^{-3}).

Applied voltage (V)	λ_s (m)	δ	Over potential (mV)	Current density (A m^{-2})
0.1	10^{-10}	0.1	0.00061	0.328
0.2	10^{-10}	0.1	0.00124	0.669
0.3	10^{-10}	0.1	0.00192	1.035
0.4	10^{-10}	0.1	0.002	1.449
0.5	10^{-10}	0.1	0.00358	1.928
0.5	10^{-8}	10	0.36	193
1	10^{-8}	10	1.14	616
1.1	10^{-8}	10	1.4	758
1.3	10^{-8}	10	2.1	1121
1.5	10^{-8}	10	2.95	1594
2	10^{-8}	10	5.64	3062
3	10^{-8}	10	7.24	3941
4	10^{-8}	10	7.27	3960
5	10^{-10}	0.1	0.073	39.2
5	10^{-9}	1	0.726	393.32
5	10^{-8}	10	7.28	3967

The calculated concentrations of four ions are used to determine the charge density that in turn appears as the source term in Eq. (11). In conclusion, a total number of five coupled and non-linear equations are simultaneously solved to model the system CaF_2–FeO. Similarly, the boundary conditions presented in Eq. (15) through Eq. (18) can be transformed and applied for the Nernst–Planck equation in the system CaF_2–FeO. For the non-reacting ions of Ca^{2+}, O^{2-}, and F^-, the total flux including electro-migration and diffusion is zero as expressed in Eqs. (15) and (16). However, the total flux is related to the current density at the anode/cathode for the reacting ferrous ion as described in Eqs. (17) and (18). Finally, the boundary conditions at the anode/cathode for Poisson equation are given in Eqs. (19) and (20). Several simulations were performed to investigate the relationship between the applied voltage, Stern layer capacitance, overpotential and current density. Table 2 summarizes the calculated results at steady state.

4.2. Boundary layer analysis

The compact diffuse layer acts like a non-linear capacitor in which the capacitance is roughly independent of concentration, but mostly dependent on the total charge. A constant capacitance for the compact layer is considered according to the well-known Stern model [14,20,24–27]. Therefore, a linear relationship can be established to describe the potential drop across the compact layer as expressed in Eq. (10). Most often, the capacitance of the compact layer is compared to the capacitance of the EDL using the ratio of effective compact layer width to Debye screening length ($\delta = \lambda_s/\lambda_D$). In the limit of small ratio ($\delta \to 0$), called Gouy–Chapman limit, the capacitance of diffuse charge layer is negligible compared to the compact layer. Consequently, the potential drop across the diffuse charge layer is dominant across the entire EDL. In contrast, in the limit of large ratio ($\delta \to \infty$), called Helmholtz limit, the capacitance of compact layer is negligible. Thus the potential drop across the compact layer accounts for the entire voltage drop across the EDL [14]. Low capacitance and subsequently large voltage drop across the Stern layer helps to drive the deposition reaction. Consequently, neither the electric field nor the concentration of the reacting ion needs to be large to sustain high current densities. It is believed that the current–voltage relation of electrochemical systems can be better predicted by using a higher ratio of δ [15]. Nevertheless, we begin our investigation of the CaF_2–FeO system considering the Gouy–Chapman limit. The first five rows of Table 2 are filled in using a low value for the ratio ($\delta = 0.1$). The calculated overpotential is notably small even though a relatively large voltage is applied. Consequently, the computed current density which is related to the overpotential through the Butler–Volmer equation, Eq. (9), is very low. Spatial variations of charge density, electric potential, and concentration of ferrous ion at different applied voltage in the range between 0.1 and 0.5 V are illustrated in Fig. 6. The electric potential field is invariant in presence or in absence of the Faradaic reaction at low applied voltage (e.g. 0.1 V) as shown in Fig. 6(a). Furthermore, the potential drop near the anode is larger than that near the cathode independent of the operational voltage. It implies that the potential field is dominantly determined by the non-reacting ions. The charge density boundary layer grows due to more deposition of ions on the surface of electrodes at higher applied voltage as illustrated in Fig. 6(b). The impact of applied voltage on the concentration profile of the ferrous ion is more pronounced. As shown Fig. 6(c), there exists a region in the vicinity of the anode where the concentration of ferrous ion increases because of higher injection rates with the increase of applied voltage. In contrast, the concentration of ferrous ion diminishes in the vicinity of the cathode due to higher removal rates at larger applied voltages.

The relationship among operational voltage and current density is strongly dependent on the ratio (δ). The last three rows of Table 2 are filled in by considering the effect of the ratio ($\delta = 0.1$, 1, or 10) on the predicted value of current density. The operational voltage (5 V) and the bulk concentration of the ferrous ion (8.96 mol m^{-3}) are kept constant. It is calculated

Please cite this article as: E. Karimi-Sibaki et al., Modeling electrochemical transport of ions in the molten CaF_2–FeO slag operating under a DC voltage, Applied Mathematics and Computation (2018), https://doi.org/10.1016/j.amc.2018.01.008

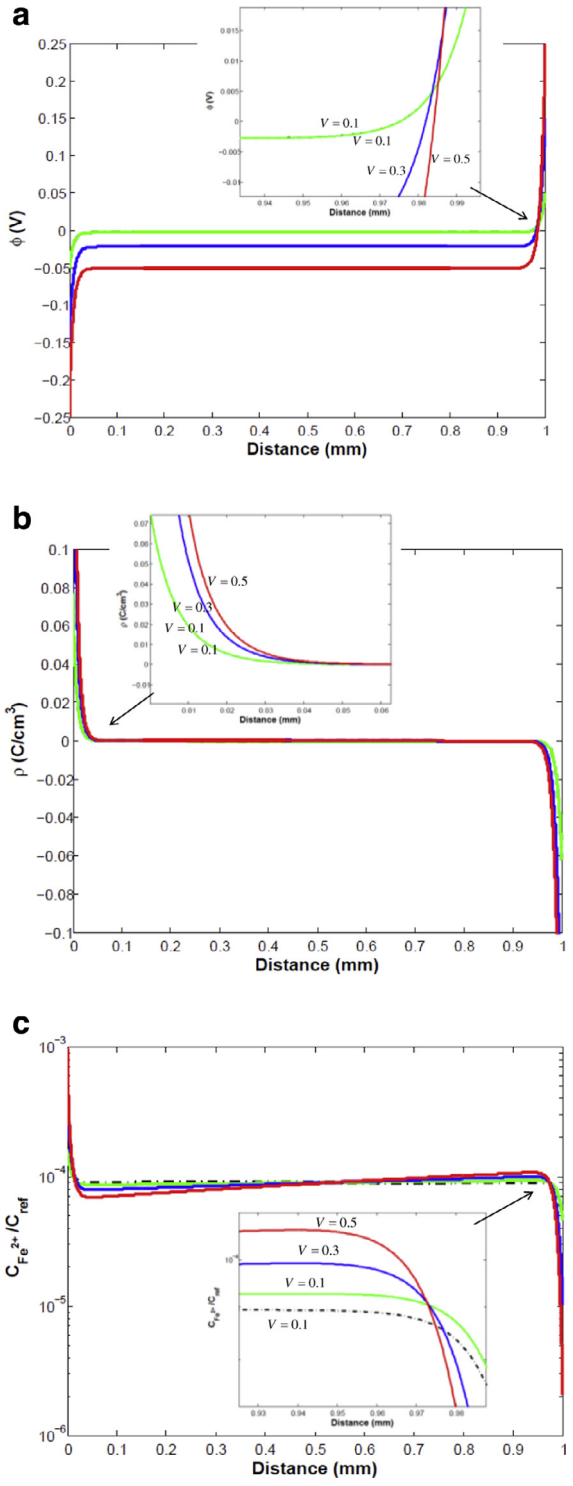

Fig. 6. The following parameters are plotted across the electrolyte (CaF_2–FeO) blocked by cathode ($x = 0$) and anode ($x = 1$) at different applied voltage using a low value for the ratio ($\delta = 0.1$), (a) electric potential, (b) charge density, (c) the dimensionless concentrations of ferrous ion. The dotted line at $V_{app} = 0.1$ V indicates field structure in absence of Faradaic reaction. Inside all plots, a zoomed area is inserted.

Please cite this article as: E. Karimi-Sibaki et al., Modeling electrochemical transport of ions in the molten CaF_2–FeO slag operating under a DC voltage, Applied Mathematics and Computation (2018), https://doi.org/10.1016/j.amc.2018.01.008

that using a high value for the ratio (e.g. $\delta = 10$) enables the system to carry a large amount of current density ($\sim$4 kA m^{-2}). However, variations in the ratio influence magnitudes of overpotential and current density through Eqs. (9) and (10) as well as rates of injection/removal of ferrous ion at anode/cathode surface through Eqs. (17) and (18). Thus, it has no influence on the spatial variation of the electric potential as shown in Fig. 7(a). In other words, the potential field remains invariant as long as the bulk concentration of the reacting ion (ferrous) remains constant.

We continue our investigation of the CaF_2–FeO system considering the Helmholtz limit by using a high value for the ratio (e.g. $\delta = 10$). The effect of operational voltage, in the range between 0.5 and 5 V, on the current-overpotential relationship is examined, and a summary of results is described in Table 2. Customarily, the overpotential as well as current density increase with the increase of operational voltage below 3 V. However, they remain almost unchanged, independent of operational voltage, above 3 V. Generally, the capacitance of EDL is limited that in turn puts a restriction on the maximum allowable current density in an electrochemical cell. Fig. 7(b) and (c) show spatial variations of electric potential and dimensionless concentration of ferrous ion across the electrolyte for three different operational voltage ($V_{app} = 0.5$, 1.1, and 1.5 V). Similar to the previous analysis using the low ratio ($\delta = 0.1$), it is observed that the interfacial potential drop near the anode is larger than that near the cathode. It implies that the potential field is essentially governed by the non-reacting ions below a certain current density ($<$1600 A m^{-2}) as long as the bulk concentration of the ferrous ion ($\sim$8.96 mol m^{-3}) is kept constant.

4.3. Confrontation between the model and an experiment

Prange et al. [34] conducted a series of experiments for the electrochemical system of CaF_2–FeO at 1723 K to investigate the kinetics of the charge transfer reaction for the ferrous ion (Fe^{2+}). Two electrodes made of solid iron as well as a crucible containing the hot slag melt were prepared. The working electrode (anode or cathode) consisted of an iron wire with 1 mm diameter. The reference electrode was an iron tube of 10 mm. Both electrodes were immersed, 7 mm deep, into slag melt. The distance between electrodes and the size of crucible (volume of slag melt) were not reported. No traces of ferric ions (Fe^{3+}) were detected in the experiment at low current density ($<$2 kA m^{-2}) indicating that oxidation of the iron at the anode, Eq. (23), and reduction of ferrous ion at the cathode, Eq. (24), are the governing redox reactions in the experiment [3,34]. Prange et al. [34] stated that the concentration polarization stays small if the double layer can be charged in a very short time. Thus, they used the double pulse technique to evaluate the relationship between the applied current density and activation (surface) overpotential. They determined a linear relationship below 1600 A m^{-2} as shown in Fig. 8. It can be seen that there is a clear tendency for overpotential to increase as time proceeds. Principally, the concentration overpotential which is created due to the presence of ion concentration gradients between the bulk of electrolyte and electrode-electrolyte interface cannot be neglected with increasing duration of time [34]. Accordingly, the activation overpotential which appears in Butler–Volmer equation, Eq. (9), is more precisely measured in a short time (e.g. 0.6 μs). Furthermore, a faster development of the concentration overpotential is expected when a higher amount of current is imposed. For instance, a noticeable difference in measured values of overpotential at different times can be seen at constant but high current density (e.g. here 1300 A m^{-2}). In the current work, we performed an extensive series of simulations to calculate the current density–overpotential relationship. As illustrated in Fig. 8, our simulation results, also reported in Table 2, are compared to the experiment. A relatively good agreement is observed below 700 A m^{-2} when the concentration overpotential stays negligibly small within the short measuring time (0.6 μs). However, the deviation between simulation results and experimental data becomes larger as the current density increases ($>$700 A m^{-2}). It appears that the accuracy of experimental data regarding to the activation overpotential notably decreases as a consequence of increase of concentration overpotential at high current density.

4.4. Beyond the model

It must be pointed out that the relationship among the current density and operational voltage is of great importance in the study of any electrochemical system. Previously, analytical solutions were derived for the current–voltage relation using the method of matched asymptotic approximation [14,15,36]. The solutions were proposed using cumbersome terms of hyperbolic trigonometric functions. Albeit, several simplifying assumptions such as limited number (two or three) with identical physical properties (e.g. charge number, concentration, and diffusion coefficient) of involving ions were made to achieve the analytical solution. Currently, we are not able to establish a current–voltage relation for the CaF_2–FeO system due to the presence of several ad hoc parameters like δ, or λ_s in the model. However, the current model greatly helped us to improve our knowledge on the electrochemical behavior of the CaF_2–FeO system subjected to a DC potential.

A desired outcome of our modeling results is that they provide insights into the basic physics. Additionally, they could be useful in interpreting experimental data which were collected during operation in several processes such as electroslag remelting (ESR). For instance, a higher melt rate was reported for the electrode-positive (anodic) compared to the electrode-negative (cathodic) for an ESR process operating under DC voltage [5,6]. The aforementioned phenomenon might be related to the contribution of non-reacting ions to the electric potential field. The Joule heating released under the electrode is proportional to the square of the electric field that in turn is directly related to the interfacial potential drop. We have shown that the interfacial potential gradient near the anode is larger than that near the cathode. Accordingly, a higher melt rate must be achieved for the electrode-positive than the electrode-negative.

Please cite this article as: E. Karimi-Sibaki et al., Modeling electrochemical transport of ions in the molten CaF_2–FeO slag operating under a DC voltage, Applied Mathematics and Computation (2018), https://doi.org/10.1016/j.amc.2018.01.008

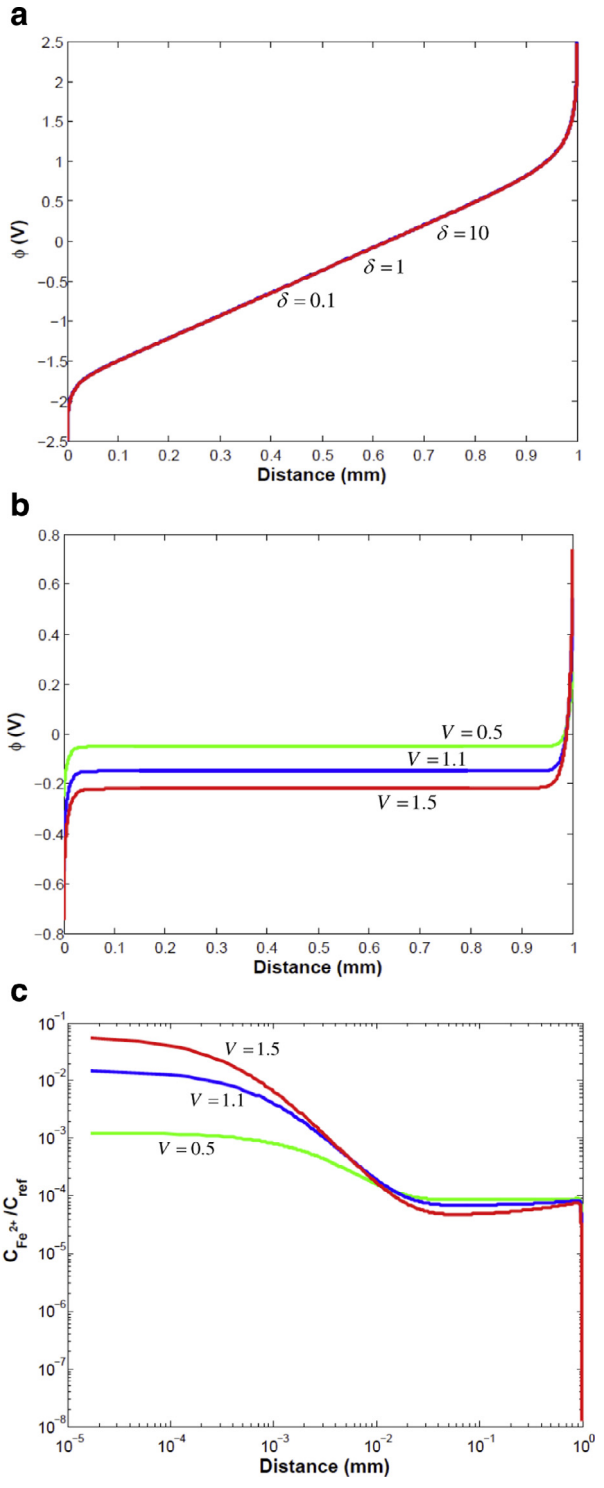

Fig. 7. The simulation results considering a fixed average concentration of ferrous ion ($C_{Fe}{}^{2+} = 8.96$ mol m^{-3}) within the electrolyte are plotted across the electrolyte (CaF_2–FeO) blocked by cathode ($x = 0$) and anode ($x = 1$): (a) electric potential field at constant applied voltage ($V_{app} = 5$ V) and using different values for the ratio ($\delta = 0.1$, 1, and 10), (b) electric potential field at constant ratio ($\delta = 10$) using different values of applied voltage ($V_{app} = 0.5$, 1.1, and 1.5 V), (c) the dimensionless concentrations of ferrous ion at constant ratio ($\delta = 10$) using different values of applied voltage ($V_{app} = 0.5$, 1.1, and 1.5 V).

Please cite this article as: E. Karimi-Sibaki et al., Modeling electrochemical transport of ions in the molten CaF_2–FeO slag operating under a DC voltage, Applied Mathematics and Computation (2018), https://doi.org/10.1016/j.amc.2018.01.008

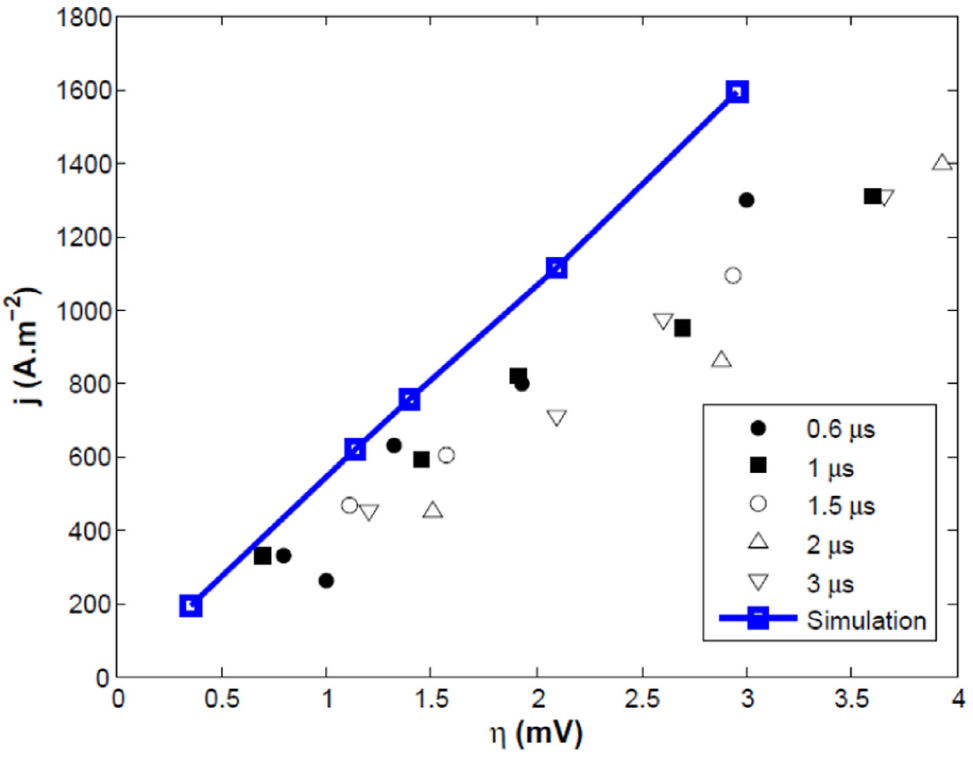

Fig. 8. The relationship among current density and activation overpotential obtained at different measuring times in the experiment conducted by Prange et al. [34] is compared with predicted results obtained by performing a series of numerical simulations. The average bulk concentration of ferrous ion was kept constant ($C_{Fe^{2+}} = 8.96$ mol m^{-3}) in both experiment and simulation. In the simulation the following parameters are used: $\lambda_s = 10^{-8}$ m, and $\delta = 10$.

In the near future, further research can be carried out on the following topics. Conventional slags used in metallurgical processes such as ESR are typically composed of CaF_2, Al_2O_3, CaO, SiO_2, MgO, etc. Accordingly, the electrochemical transport of other ions like Al^{3+}, Si^{4+}, and Mg^{2+} must be included into the current model. Furthermore, the effect of bulk concentration of reacting ions such as Fe^{2+} on the current–overpotential relationship requires further investigation. Conventionally, the presence of excess of non-reacting ions (called supporting electrolyte) permitted a simplification in the analysis. Concentration gradients for the non-reacting ions had been thus far neglected, allowing for the assumption of a constant electrical conductivity (using Ohm's law) for the well-mixed electrolyte [17]. In the presence of flow, concentrations of ions near electrodes differ significantly from their bulk values. The flow may sufficiently promote stirring, so that the concentration field becomes uniform in the bulk of electrolyte. As such, the advective transport of ions in the bulk of molten slag must be included in the future model as it has a crucial role in industrial electrochemical processes [12,17,30,37,38].

5. Summary

A numerical study is performed to investigate the electrochemical transport of ions in the molten slag made of CaF_2–FeO at 1723 K. A one-dimensional model is proposed to study the electrochemical system including two parallel and planar electrodes separated by the fully dissociated electrolyte. The electrochemical transport of ions including diffusion and electro-migration are modeled by solving the coupled Poisson–Nernst–Planck (PNP) equations. Furthermore, Faradaic reactions which occur on the electrode-electrolyte interface are taken into account by implementing the well-known Butler–Volmer equation. Firstly, we studied the electrochemical behavior of a binary symmetrical electrolyte (ZZ) involving reacting Z^+ and inert Z^- ions. This study solely aims at demonstrating the capability of our model to capture key phenomena which were presented in the past by other researchers. Secondly, we applied the model to study the electrochemical behavior of the fully dissociated CaF_2–FeO slag composed of Ca^{+2}, F^-, Fe^{+2} and O^{2-} ions. The Faradaic reactions of the ferrous ion (Fe^{+2}) electrode–slag interface is taken into account. The electric double layer (EDL) that appears on the surface of electrode is consisted of Stern layer, diffusion layer, and diffuse charge layer. The ratio of effective Stern layer width to Debye screening length is denoted δ. The chosen value of δ determines the potential drop across the Stern layer. The following conclusions are made:

- In the limit of small ratio (e.g. $\delta = 0.1$), low amount of current density ($\sim$1 A m^{-2}) flows through the cell. It is found that the Faradaic reaction of the ferrous ion has no influence on the electric potential field which is completely determined by non-reacting ions. Furthermore, the potential drop near the anode is larger than that near the cathode.

Please cite this article as: E. Karimi-Sibaki et al., Modeling electrochemical transport of ions in the molten CaF_2–FeO slag operating under a DC voltage, Applied Mathematics and Computation (2018), https://doi.org/10.1016/j.amc.2018.01.008

- With the increase of applied voltage, the concentration of ferrous ion in the vicinity of anode increases whereas the concentration decreases nearby the cathode when very low amount of current density (<1 A m^{-2}) is imposed.
- The effective Stern layer width and subsequently δ is an ad hoc parameter. However, it is found that these parameters have no influence on the profile of the electric potential as long as the total amount of the reacting ferrous ion within the electrolyte is kept constant.
- In the limit of large ratio (e.g. $\delta = 10$), substantial amount of current density ($\sim$3 kA m^{-2}) can flow through the cell at low applied voltage ($\sim$2 V). Once again, it is observed that the interfacial potential drop near the anode is larger than that near the cathode.
- Previously, experimental measurements revealed a linear relationship among activation overpotential and current density below 1600 A m^{-2}. We performed an extensive series of simulations to investigate the aforementioned linear relationship. The simulation results were examined against the experiment.

Although the current study is purely fundamental research, the obtained results enable us to propose possible explanation for some phenomena which were observed in several metallurgical processes such as electroslag remelting (ESR) during operation. For instance, the stronger potential drop near the anode than that near the cathode due to the contribution of non-reacting ions to the electric potential field may alter the thermal field adjacent to the electrode. Note that, the Joule heating provided to the process which governs the melt rate of the electrode in the ESR process is directly proportional to the potential drop. Accordingly, a higher melt rate of electrode for electrode-positive (anodic) than the electrode-negative (cathodic) is expected that was in-situ observed in the ESR process during actual operation.

Acknowledgments

The authors acknowledge the financial support by the Austrian Federal Ministry of Economy, Family and Youth and the National Foundation for Research, Technology and Development within the framework of the Christian Doppler Laboratory for Advanced Process Simulation of Solidification and Melting.

References

[1] A. Allanore, Features and challenges of molten oxide electrolytes for metal extraction, J. Electrochem. Soc. 162 (1) (2015) E13–E22.
[2] M.E. Peover, Electroslag remelting: a review of electrical and electrochemical aspects, J. Inst. Metals 100 (1972) 97–106.
[3] A. Mitchell, G. Beynon, Electrode polarization in the DC electroslag melting of pure iron, Metall. Trans. 2 (1971) 3333–3345.
[4] A. Mitchell, J. Cameron, The electrical conductivity of some liquids in the system CaF_2+CaO+Al_2O_3, Metall. Trans. 2 (1971) 3361–3366.
[5] Y. Kojima, M. Kato, T. Toyoda, M. Inouye, On the droplet formation at the tip of electrode by DC ESR with small scale unit, Trans. ISIJ 15 (1975) 394–406.
[6] M. Kawakami, K. Nagata, M. Yamamura, N. Sakata, Y. Miyashita, K.S. Goto, Profiles of temperature, voltage and local heat generation in slag phase and metal pool of ESR unit under operation, Testsu-to-Hagane 63 (1977) 2162–2171.
[7] E. Karimi-Sibaki, A. Kharicha, J. Bohacek, M. Wu, A. Ludwig, A dynamic mesh-based approach to model melting and shape of an ESR electrode, Metall. Mater. Trans. B 46 (2015) 2049–2061.
[8] A. Kharicha, M. Wu, A. Ludwig, A. Ramprecht, H. Holzgruber, Influence of the frequency of the applied AC current on the electroslag remelting process, CFD Modeling and Simulation in Materials Processing, Wiley–Interscience, New York, 2012.
[9] A. Kharicha, M. Wu, A. Ludwig, E. Karimi-Sibaki, Simulation of the electric signal during the formation and departure of droplets in the electroslag remelting process, Metall. Mater. Trans. B 47 (2016) 1427–1434.
[10] M. Etienne, The Loss of Reactive Elements During Electroslag Processing of Iron-based Alloys Ph.D. Thesis, University of British Columbia (UBC), 1971.
[11] N.Q. Minh, T.B. King, The contribution of electrochemical reactions to sulfur transfer from electrode to slag in electroslag remelting, Metall. Trans. B 10 (1979) 623–629.
[12] W. Pongsaksawad, A.C. Powell IV, D. Dussault, Phase-field modeling of transport-limited electrolysis in solid and liquid states, J. Electrochem. Soc. 154 (6) (2007) F122–F133.
[13] E. Karimi-sibaki, A. Kharicha, M. Wu, A. Ludwig, A numerical study on electrochemical transport of ions in calcium fluoride slag, IOP Conf. Ser. Mater. Sci. Eng. 143 (2016) 012008, doi:10.1088/1757-899X/143/1/012008.
[14] M.Z. Bazant, K.T. Chu, B.J. Bayly, Current–voltage relations for electrochemical thin films, SIAM J. Appl. Math. 65 (2005) 1463–1484.
[15] K.T. Chu, M.Z. Bazant, Electrochemical thin films at and above the classical limiting current, SIAM J. Appl. Math. 65 (2005) 1485–1505.
[16] A. Golovnev, S. Trimper, Steady state solution of Poisson–Nernst–Planck equations, Phys. Lett. A 374 (2010) 2886–2889.
[17] J. Newman, K.E. Thomas-Alyea, Electrochemical Systems, John Wiley & Sons, New Jersey, 2004.
[18] A.D. McNaught, A. Wilkinson, IUPAC Compendium of Chemical Terminology, second ed., Blackwell Scientific Publications, Oxford, 1997.
[19] K.T. Chu, Asymptotic Analysis of Extreme Electrochemical Transport (Ph.D.) Thesis, Massachusetts Institute of Technology (MIT), 2005.
[20] E.M. Itskovich, A.A. Kornyshev, M.A. Vorotyntsev, Electric current across the metal-solid electrolyte interface. I. Direct current, current–voltage characteristic, Phys. Stat. Sol. 39 (1977) 229–238.
[21] A. Bonnefont, F Argoul, M.Z. Bazant, Analysis of diffuse-layer effects on time-dependent interfacial kinetics, J. Electroanal. Chem. 500 (2001) 52–61.
[22] P.M. Biesheuvel, M. Van Soestbergen, M.Z. Bazant, Imposed currents in galvanic cells, Electrochim. Acta 54 (2009) 4857–4871.
[23] B. Van Leer, Toward the ultimate conservative difference scheme. V. A second-order sequel to Godunov's method, J. Comput. Phys. 32 (1979) 101–136.
[24] M.Z. Bazant, K. Thornton, A. Ajdari, Diffuse-charge dynamics in electrochemical systems, Phys. Rev. E. 70 (2004) 021506.
[25] I. Rubinstein, B. Shtilman, Voltage against current curves of cation exchange membranes, J. Chem. Soc. Faraday Trans. II 75 (1979) 231–246.
[26] J. Newman, The polarized diffuse double layer, Trans. Faraday Soc. 61 (1965) 2229–2237.
[27] W.H. Smyrl, J. Newman, Double layer structure at the limiting current, Trans. Faraday Soc. 63 (1967) 231–246.
[28] V.S. Pham, Z. Li, K.M. Lim, J.K. White, J. Han, Direct numerical simulation of electroconvective instability and hysteretic current-voltage response of a permselective membrane, Phys. Rev. E 86 (2012) 046310.
[29] N. Ariel, G. Ceder, D.R. Sadoway, E.A. Fitzgerald, Electrochemically controlled transport of lithium through ultrathin SiO_2, J. Appl. Phys. 98 (2005) 023516.
[30] A. Allanore, Electrochemical engineering of anodic oxygen evolution in molten oxides, Electrochim. Acta 110 (2013) 587–592.
[31] N.F. Mott, Conduction in glasses containing transition metal ions, J. Non-Cryst. Solids 1 (1968) 1–17.
[32] M. Barati, K.S. Coley, Electrical and electronic conductivity of CaO–SiO_2–FeO_x slags at various oxygen potentials: Part II. Mechanism and a model of electronic conduction, Metall. Mater. Trans. B 37 (2006) 51–60.

Please cite this article as: E. Karimi-Sibaki et al., Modeling electrochemical transport of ions in the molten CaF_2–FeO slag operating under a DC voltage, Applied Mathematics and Computation (2018), https://doi.org/10.1016/j.amc.2018.01.008

[33] W. Chiho, X. Shunhua, Electrical conductivity of Molten slags of CaF_2+Al_2O_3 and CaF_2+Al_2O_3+CaO systems for ESR, ISIJ Int. 33 (1993) 239–244.
[34] R. Prange, K. Heusler, K. Schwerdtfeger, Charge transfer at Fe/FeO (CaF_2) electrodes at 1450 °C: exchange current density, electrode capacitance, diffusivity, Metall. Trans. B 15 (1984) 281–288.
[35] M. Allibert, H. Gaye, J. Geiseler, D. Janke, B.J. Keene, D. Kirner, M. Kowalski, J. Lehmann, K.C. Mills, D. Neuschütz, R. Parra, C. Saint-Jours, P.J. Spencer, M. Susa, M. Tmar, E. Woermann, Slag Atlas, Verlag Stahleisen GmbH, Düsseldorf, Germany, 1995.
[36] E. Yariv, Y. Almog, Ionic currents in the presence of supporting electrolytes, Phys. Rev. Lett. 105 (2010) 176101.
[37] E. Karimi-Sibaki, A. Kharicha, M. Wu, A. Ludwig, and J. Bohacek, Toward modeling of electrochemical reactions during electroslag remelting (ESR) process. Steel Res. Int. 88 (2017) 1700011. doi:10.1002/srin.201700011.
[38] A.H. Caldwell, E. Lai, A.J. Gmitter, A. Allanore, Influence of mass transfer and electrolyte composition on anodic oxygen evolution in molten oxides, Electrochim. Acta 219 (2016) 178–186.

Please cite this article as: E. Karimi-Sibaki et al., Modeling electrochemical transport of ions in the molten CaF_2–FeO slag operating under a DC voltage, Applied Mathematics and Computation (2018), https://doi.org/10.1016/j.amc.2018.01.008